Geophysical Journal International

Geophys. J. Int. (2014) **197,** 1527–1531
Advance Access publication 2014 April 24

doi: 10.1093/gji/ggu093

EXPRESS LETTER

Source and processing effects on noise correlations

Andreas Fichtner

Department of Earth Sciences, ETH Zurich, Switzerland. E-mail: andreas.fichtner@erdw.ethz.ch

Accepted 2014 March 11. Received 2014 March 9; in original form 2014 February 6

SUMMARY

We quantify the effects of spatially heterogeneous noise sources and seismic processing on noise correlation measurements and their sensitivity to Earth structure. Using numerical wavefield simulations and adjoint techniques, we calculate interstation correlations and sensitivity kernels for arbitrarily distributed noise sources where—as in the real Earth—different frequencies are generated in different locations. While both heterogeneous noise sources and processing can have profound effects on noise correlation waveforms, narrow-band traveltime measurements are less affected, in accord with previous analytical studies. Sensitivities to Earth structure depend strongly on the source distribution and the processing scheme, and they reveal exotic frequency dependencies that go beyond the well-known frequency scaling of the Fresnel zone width. Our results indicate that modern full waveform inversion applied to noise correlations is not possible unless one of the following measures is taken: (1) properly account for noise source distribution and processing, or (2) limit measurements to phase or time shifts in narrow frequency bands. Failure to do so can lead to erroneous misfits, tomographic artefacts, and reduced resolution.

Key words: Inverse theory; Tomography; Interferometry; Computational seismology.

GJI Seismology

1 INTRODUCTION

Following contributions of Shapiro *et al.* (2005) and Sabra *et al.* (2005), seismic tomography based on ambient noise correlations has become standard. The method, frequently referred to as 'noise tomography', rests on the assumed equality of noise correlations and Green's functions, from which information on Earth structure can be extracted. This assumption, however, only holds under special conditions, including wavefield diffusivity and equipartitioning (e.g. Lobkis & Weaver 2001; Sánchez-Sesma & Campillo 2006), or the isotropic distribution of both mono- and dipolar uncorrelated noise sources (e.g. Wapenaar 2004).

Since none of these conditions is satisfied in the Earth, various processing steps are commonly applied to obtain 'good' Green's function estimates. Examples include one-bit normalization, spectral-whitening, averaging causal and anticausal parts and many others (e.g. Bensen *et al.* 2007). The choice of processing is to some degree subjective; and it depends on the data and the type of information that one wishes to extract (e.g. surface-wave dispersion or body-wave arrival times). Both the heterogeneous distribution of noise sources and the processing affect the details of noise correlations and their sensitivity to Earth structure.

With the advent of full waveform inversion (FWI) methods (e.g. Tape *et al.* 2010; Fichtner *et al.* 2013) and the noise-based monitoring of time-dependent Earth structure (e.g. Brenguier *et al.* 2008), these details have acquired a new level of relevance. Powerful optimization schemes in FWI can map small waveform differences into spurious Earth structure, and the time dependence of correlations related to noise source variations may be misinterpreted as subsurface changes.

While source effects on noise correlations are well understood (e.g. Tsai 2009; Tromp *et al.* 2010), the purpose of this paper is to go one step beyond and to quantify the effects of both heterogeneous noise sources and seismic processing on noise correlations and their sensitivity to Earth structure. Given the plethora of data- and application-specific scenarios, we have decided to focus on the physics of the problem, and to describe a limited number of illustrative examples that allow us to draw conclusions that are as general as possible.

2 EFFECTS OF PROCESSING AND HETEROGENEOUS NOISE SOURCES ON MEASUREMENTS

We start our analysis with a description of noise correlation modelling with spatially heterogeneous noise sources where different frequencies are generated in different locations. This will be followed, in Section 2.2, by examples where we compute biases in narrow-band traveltime and time-frequency phase measurements, induced by heterogeneous sources and the optional spectral whitening prior to correlation.

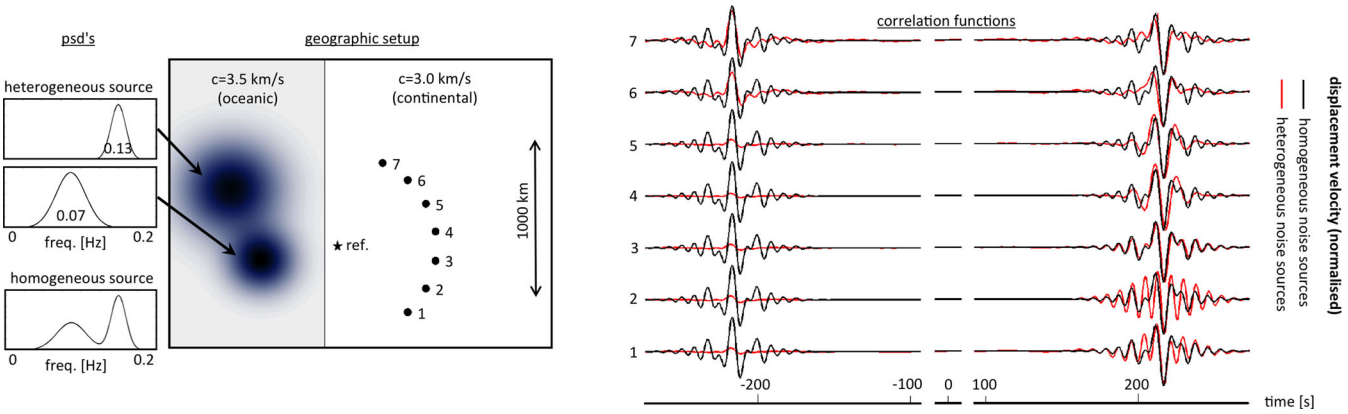

Figure 1. Left-hand panel: medium properties and receiver geometry. The domain consists of two parts with $c = 3.5$ km s^{-1} and $c = 3.0$ km s^{-1}, respectively. Seven receivers (circles) are placed at equal distances from the reference station (star). Gaussian-shaped heterogeneous noise sources are shown in blue, with their respective power-spectral densities shown to the left. Right-hand panel: correlation functions for the homogeneous (black) and heterogeneous (red) source distributions.

2.1 Noise correlation modelling

To emphasize the physics of the problem, we limit ourselves to acoustics, that is, to wavefields $u(\mathbf{x}, \omega)$ governed by the acoustic wave equation

$$\mathcal{L}u(\mathbf{x}, \omega) = -\omega^2\, u(\mathbf{x}, \omega) - c^2(\mathbf{x})\Delta u(\mathbf{x}, \omega) = N(\mathbf{x}, \omega)\,. \qquad (1)$$

In eq. (1), $\mathcal{L}$, c and N denote the wave equation operator, the acoustic wave speed and the noise source distribution, respectively. The modelling of ambient noise correlations is most easily derived in the frequency domain, where the representation theorem is given by

$$u(\mathbf{x}) = \int G(\mathbf{x}, \boldsymbol{\xi})\, N(\boldsymbol{\xi})\, \mathrm{d}\boldsymbol{\xi}\,, \qquad (2)$$

with $G(\mathbf{x}, \boldsymbol{\xi})$ being the Green's function with source at position $\boldsymbol{\xi}$. Dependencies of u, G and N on the circular frequency ω are omitted in the interest of a condensed notation. Using (2), the correlation of recordings at positions $\mathbf{x}_1$ and $\mathbf{x}_2$ takes the form

$$\begin{aligned} \mathcal{C}(\mathbf{x}_1, \mathbf{x}_2) &= u(\mathbf{x}_1) u^*(\mathbf{x}_2) \\ &= \iint G(\mathbf{x}_1, \boldsymbol{\xi}_1) G^*(\mathbf{x}_2, \boldsymbol{\xi}_2)\, N(\boldsymbol{\xi}_1) N^*(\boldsymbol{\xi}_2)\, \mathrm{d}\boldsymbol{\xi}_1\, \mathrm{d}\boldsymbol{\xi}_2\,, \end{aligned} \qquad (3)$$

where $*$ denotes complex conjugation. Following Woodard (1997), we compute the expectation $\langle\,.\,\rangle$ of (3), and assume that noise sources are spatially uncorrelated in the sense that $\langle N(\boldsymbol{\xi}_1) N^*(\boldsymbol{\xi}_2)\rangle = S(\boldsymbol{\xi}_1)\,\delta(\boldsymbol{\xi}_1 - \boldsymbol{\xi}_2)$, with the power-spectral density (psd) S. Taking into account that Green's functions do not change over time, the expected noise correlation now takes the form of a single integral over space:

$$C(\mathbf{x}_1, \mathbf{x}_2) = \langle \mathcal{C}(\mathbf{x}_1, \mathbf{x}_2)\rangle = \int G(\mathbf{x}_1, \boldsymbol{\xi}) G^*(\mathbf{x}_2, \boldsymbol{\xi})\, S(\boldsymbol{\xi})\, \mathrm{d}\boldsymbol{\xi}\,. \qquad (4)$$

Comparing (2) and (4), we note that $C(\mathbf{x}_1, \mathbf{x}_2)$ can be understood as a 'correlation wavefield'

$$C(\mathbf{x}, \mathbf{x}_2) = \int G(\mathbf{x}, \boldsymbol{\xi})\, [G^*(\mathbf{x}_2, \boldsymbol{\xi})\, S(\boldsymbol{\xi})]\, \mathrm{d}\boldsymbol{\xi}\,, \qquad (5)$$

evaluated at position $\mathbf{x} = \mathbf{x}_1$, and excited by the deterministic source $G^*(\mathbf{x}_2, \boldsymbol{\xi})\, S(\boldsymbol{\xi})$. Eq. (5) provides a recipe for the calculation of expected correlations at any position $\mathbf{x}$ and a reference station at position $\mathbf{x}_2$. Illustrations of the correlation wavefield can be found in the Supporting Information.

2.2 Measurement biases in traveltimes and time–frequency phase differences

To compute correlations for heterogeneous media and source distributions, we use 2-D finite-differences. As illustrated in Fig. 1, the computational domain is split into two parts, with velocities approximating the phase velocity of Rayleigh waves at 10 s period in oceanic ($c = 3.5$ km s^{-1}) and continental ($c = 3.0$ km s^{-1}) regions, respectively. Seven receivers at equal distance from a reference station are placed on the continental side. All boundaries are absorbing.

We perform three types of simulations: (1) To establish a reference, we compute correlations for a homogeneous source distribution and a psd with peaks at 0.07 Hz and 0.13 Hz (Fig. 1, left-hand panel). The correlations are shown in black in Fig. 1(right-hand panel). (2) To mimick the one-sided illumination typical for coastal regions, we place two source regions on the oceanic side. Their psd's peak at 0.07 and 0.13 Hz, roughly representing primary and secondary microseisms, respectively. Superimposed is a weak homogeneous source with a psd as in the previous scenario. The correlations are shown in red in Fig. 1(right-hand panel). (3) Finally, correlations for spectrally whitened noise are computed by replacing the original psd $S(\boldsymbol{\xi})$ by the new effective psd $S(\boldsymbol{\xi})/[|u(\mathbf{x_1})||u(\mathbf{x_2})|]$. Examples are shown in Fig. 2 (right-hand panel).

The correlations computed for these scenarios reveal large differences. To assess their impact on a hypothetical traveltime tomography, we compute frequency-dependent cross-correlation traveltime shifts (Luo & Schuster 1991) between the reference correlations and the correlations for geographically heterogeneous sources. These traveltime shifts, which should ideally be zero, are a proxy for traveltime biases induced by heterogeneous noise sources. Results for the frequency bands 0.06–0.08 and 0.14–0.16 Hz are summarized in Fig. 2 (left-hand panel). Traveltime biases are on the order of ± 1 s, and strongly position- and frequency-dependent. However, the effect of subjective choices (measuring/averaging causal or anticausal parts, spectral whitening) is less than 0.1 s for a given station and frequency band.

While the bias in narrow-band traveltimes is relatively small, measurements with a higher time resolution—frequently used in FWI—suffer substantially. These include time-domain waveform misfits (e.g. Brossier *et al.* 2009) and time–frequency phase differences (Fichtner *et al.* 2008, 2013), for which examples are shown in

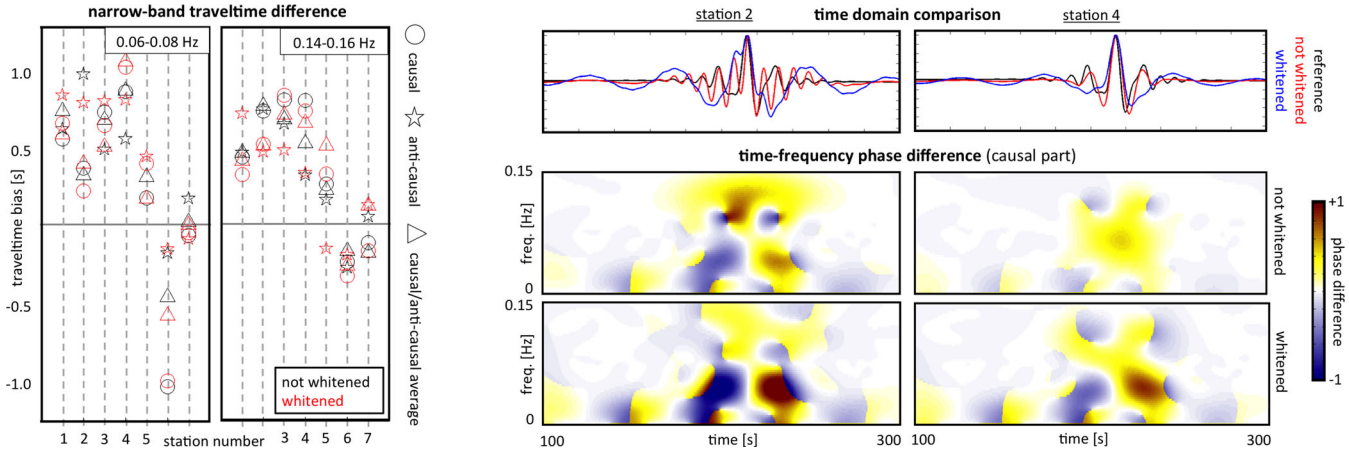

Figure 2. Left-hand panel: traveltime bias measured by cross-correlation in the frequency bands 0.06–0.08 and 0.14–0.16 Hz for non-whitened (black) and whitened (red) noise. Measurements were made on the causal (circle), anti-causal (star), and the averaged causal/anti-causal (triangle) correlations. Right-hand panel: comparison at stations 2 and 4 of the causal parts of the reference (black), non-whitened (red) and whitened (blue) correlations in terms of time-domain waveforms (top) and time–frequency phase differences (below).

Fig. 2 (right-hand panel). Furthermore, these biases strongly depend on whether spectral whitening is applied or not. Animations of the correlation wavefields for the previously discussed scenarios can be found in the Supporting Information.

3 EFFECTS OF PROCESSING AND HETEROGENEOUS NOISE SOURCES ON STRUCTURAL SENSITIVITY

To quantify source and processing effects on sensitivity to Earth structure, we compute sensitivity kernels for noise correlation measurements. In Section 3.1, we propose a derivation of noise correlation sensitivities that is more compact than the one provided by Tromp *et al.* (2010). This will be followed in Section 3.2 by examples of source- and processing-dependent sensitivities for finite-frequency traveltime measurements.

3.1 Computing sensitivity kernels

As a result of the chain rule, we can write the first variation of a measurement $\chi(C)$ with respect to earth model parameters $\mathbf{m}(\mathbf{x})$ as

$$\delta\chi = \mathrm{Re}\int \delta C(\mathbf{x}_1,\mathbf{x}_2,\omega)\, f(\omega)\,\mathrm{d}\omega\,, \tag{6}$$

where the specific form of f depends on the definition of χ (see Section 3.2 for examples). Introducing into (6) the first variation of $C(\mathbf{x}_1,\mathbf{x}_2,\omega)$ from eq. (4), gives the variation of the measurement χ in terms of the variation of Green's functions:

$$\delta\chi = \mathrm{Re}\iint G(\mathbf{x}_1,\boldsymbol{\xi})\delta G^*(\mathbf{x}_2,\boldsymbol{\xi})S(\boldsymbol{\xi})f\,\mathrm{d}\boldsymbol{\xi}\,\mathrm{d}\omega + \mathrm{Re}\iint \delta G(\mathbf{x}_1,\boldsymbol{\xi})G^*(\mathbf{x}_2,\boldsymbol{\xi})S(\boldsymbol{\xi})f\,\mathrm{d}\boldsymbol{\xi}\,\mathrm{d}\omega\,. \tag{7}$$

Denoting by $G^\dagger$ the adjoint Green's function, we invoke Green's theorem (e.g. Hanasoge *et al.* 2011)

$$\delta G(\mathbf{x}_1,\boldsymbol{\xi}) = -\int G^\dagger(\mathbf{x},\mathbf{x}_1)\,[\delta\mathcal{L}G(\mathbf{x},\boldsymbol{\xi})]\,\mathrm{d}\mathbf{x}\,, \tag{8}$$

to transform (7) into a sequence of products of forward and adjoint Green's functions:

$$\delta\chi = -\mathrm{Re}\iiint \big[G^{\dagger *}(\mathbf{x},\mathbf{x}_2)\,G(\mathbf{x}_1,\boldsymbol{\xi})\,[\delta\mathcal{L}^*G^*(\mathbf{x},\boldsymbol{\xi})]\,S(\boldsymbol{\xi}) + G^*(\boldsymbol{\xi},\mathbf{x}_2)G^\dagger(\mathbf{x},\mathbf{x}_1)[\delta\mathcal{L}G(\mathbf{x},\boldsymbol{\xi})]S(\boldsymbol{\xi})\big]\,f\,\mathrm{d}\mathbf{x}\,\mathrm{d}\boldsymbol{\xi}\,\mathrm{d}\omega. \tag{9}$$

Isolating integrals over $\boldsymbol{\xi}$, we identify the correlation fields $C^*(\mathbf{x},\mathbf{x}_1)$ and $C(\mathbf{x},\mathbf{x}_2)$ in (9), allowing us to condense the expression for $\delta\chi$ to

$$\delta\chi = -\mathrm{Re}\iint u^\dagger(\mathbf{x},\mathbf{x}_2)\,[\delta\mathcal{L}C(\mathbf{x},\mathbf{x}_1)]\,\mathrm{d}\mathbf{x}\,\mathrm{d}\omega - \mathrm{Re}\iint u^\dagger(\mathbf{x},\mathbf{x}_1)\,[\delta\mathcal{L}C(\mathbf{x},\mathbf{x}_2)]\,\mathrm{d}\mathbf{x}\,\mathrm{d}\omega, \tag{10}$$

with the adjoint fields $u^\dagger(\mathbf{x},\mathbf{x}_2)$ and $u^\dagger(\mathbf{x},\mathbf{x}_1)$ defined as

$$u^{\dagger *}(\mathbf{x},\mathbf{x}_2) = G^\dagger(\mathbf{x},\mathbf{x}_2)\,f^* \quad \text{and} \quad u^\dagger(\mathbf{x},\mathbf{x}_1) = G^\dagger(\mathbf{x},\mathbf{x}_1)\,f\,. \tag{11}$$

From eq. (1) we see that the variation of $\mathcal{L}$ with respect to velocity c is $\delta\mathcal{L} = -2c\delta c\,\Delta$. Substituting this result into (10), gives

$$\delta\chi = \int K(\mathbf{x})\,\delta c(\mathbf{x})\,\mathrm{d}\mathbf{x}\,, \tag{12}$$

with the sensitivity kernel

$$K(\mathbf{x}) = 2c(\mathbf{x})\,\mathrm{Re}\int \big[u^\dagger(\mathbf{x},\mathbf{x}_2)\,\Delta C(\mathbf{x},\mathbf{x}_1) + u^\dagger(\mathbf{x},\mathbf{x}_1)\,\Delta C(\mathbf{x},\mathbf{x}_2)\big]\,\mathrm{d}\omega\,. \tag{13}$$

The calculation of $K(\mathbf{x})$ requires 4 forward simulations for the Green's functions $G(\mathbf{x},\mathbf{x}_1)$ and $G(\mathbf{x},\mathbf{x}_2)$, and the correlation fields $C(\mathbf{x},\mathbf{x}_1)$ and $C(\mathbf{x},\mathbf{x}_2)$, plus two adjoint simulations for $u^\dagger(\mathbf{x},\mathbf{x}_1)$ and $u^\dagger(\mathbf{x},\mathbf{x}_2)$. Examples are given in the following section.

3.2 Source- and processing-dependent sensitivity of finite-frequency traveltimes

We compute sensitivity kernels under the assumption that the noise source is known and that processing—in our examples in the form of spectral whitening—is correctly taken into account. Our measurements are frequency-dependent traveltimes determined by

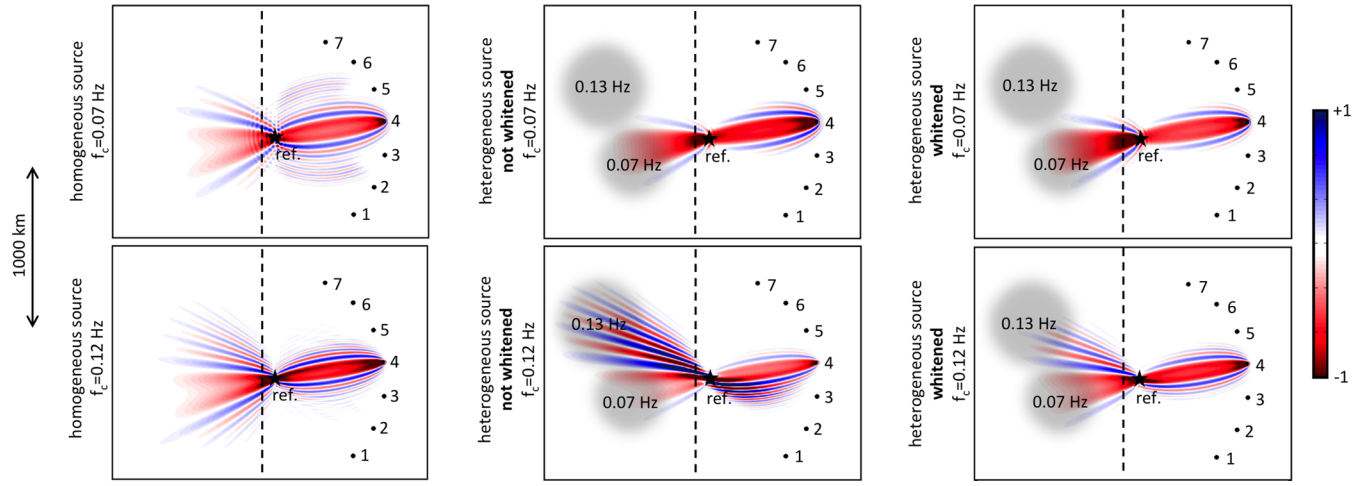

Figure 3. Normalized sensitivities $K(\mathbf{x})$, for traveltimes at frequencies of 0.07 ± 0.02 Hz (top) and 0.12 ± 0.02 Hz (bottom) measured on the causal part of the correlations. Left-hand panel: homogeneous source distribution. Centre panel: heterogeneous source distribution as shown in Fig. 1, 'without' spectral whitening. Right-hand panel: as in the centre, but 'with' spectral whitening. The heterogeneous source is marked by grey shading, with dominant frequencies indicated.

cross-correlation, for which f in eq. (6) is equal to $i\omega C / \int \omega^2 |C|^2 d\omega$ (e.g. Luo & Schuster 1991; Dahlen *et al.* 2000). Fig. 3 shows sensitivity kernels for measurements at frequencies around 0.07 and 0.12 Hz on the causal part of the correlations between the reference station and station 4. Kernels for the homogeneous source distribution are displayed to the left, and kernels for the heterogeneous source distribution from Fig. 1 are shown in the centre ('without' spectral whitening) and to the right ('with' spectral whitening).

In addition to the classical Fresnel zone connecting the two receivers, high sensitivity extends far left of the reference station. This feature does not exist for standard source-receiver geometries. A comparison of the different scenarios in Fig. 3 reveals that the shape of the sensitivity kernels is strongly affected by the noise source distribution, as noted already by Tromp *et al.* (2010). Spectral whitening effectively changes the noise source distribution, and therefore has a strong effect on the sensitivities as well.

4 DISCUSSION AND CONCLUSIONS

We study the effects of heterogeneous noise sources and processing on noise correlation measurements and their sensitivity to Earth structure. In accord with analytical approaches (e.g. Tsai 2009; Froment *et al.* 2010), we find that traveltimes measured in narrow frequency bands are weakly affected by noise source heterogeneity, with errors of ∼1 s over 500 km distance. The effect of processing (spectral whitening, measuring at positive or negative time lags) on narrow-band traveltimes is practically negligible. This explains the similarity of earthquake and noise tomographies based on similar measurements (e.g. Lin *et al.* 2008; Shen *et al.* 2013). Nevertheless, these measurement biases are relevant in monitoring applications.

While narrow-band traveltimes are robust, correlation waveforms are strongly affected by the source distribution and the processing that modifies the effective sources. This is consistent with the work of Halliday & Curtis (2008), Kimman & Trampert (2010) and Cobden *et al.* (2010). It follows that misfit measures with higher time resolution such as time-domain waveform misfits or time–frequency phase difference (Fig. 2) are hardly meaningful when noise sources and processing are not accounted for correctly. This implies that FWI schemes (e.g. Tape *et al.* 2010; Fichtner *et al.* 2013), when applied to noise correlations, should either reduce the exploited information to narrow-band traveltimes, or properly account for all factors contributing to the details of noise correlation waveforms.

As illustrated in Fig. 3, noise source characteristics strongly affect sensitivity to Earth structure. Since processing modifies the effective noise source, it leaves an imprint on structural sensitivity as well, and we illustrated this effect using the example of spectral whitening. Seismic noise at different frequencies is generated in different locations, with considerable variation existing already within the narrow secondary microseism band (Ardhuin *et al.* 2011). This complexity introduces an additional frequency dependence of sensitivity kernels that goes beyond the well-know frequency scaling of the Fresnel zone width.

Ignoring source and processing effects, will—as in earthquake tomography—slow down the convergence of optimization schemes, and potentially lead to tomographic artefacts (Hanasoge 2014). Correctly modelling the fine structure of sensitivity kernels has the potential to significantly improve tomographic resolution. This potential, which motivates the calculation of finite-frequency kernels, should in the future also be used for seismic tomography based on interstation ambient noise correlations.

ACKNOWLEDGEMENTS

I would like to thank Michael Afanasiev, Moritz Bernauer, Laura Cobden, Laura Ermert, Lucia Gualtieri, Shravan Hanasoge and Victor Tsai for comments and discussions that helped me to improve this manuscript.

REFERENCES

Ardhuin, F., Stutzmann, E., Schimmel, M. & Mangeney, A., 2011. Ocean wave sources of seismic noise, *J. geophys. Res.* **116,** doi:10.1029/2011JC006952.

Bensen, G. D., Ritzwoller, M.H., Barmin, M.P., Levshin, A.L., Lin, F., Moschetti, M.P., Shapiro, N. M. & Yang, Y., 2007. Processing seismic ambient noise data to obtain reliable broad-band surface wave dispersion measurements, *Geophys. J. Int.* **169,** 1239–1260.

Brenguier, F., Campillo, M., Hazioannou, C., Shapiro, N.M., Nadeau, R.M. & Larose, E., 2008. Postseismic relaxation along the San Andreas fault at Parkfield from continuous seismological observations, *Science* **321,** 1478–1481.

Brossier, R., Operto, S. & Virieux, J., 2009. Seismic imaging of complex onshore structures by 2D elastic frequency-domain full-waveform inversion, *Geophysics* **74,** WCC105–WCC118.

Cobden, L.J., Tong, C.H. & Warner, M.R., 2010. Influence of acoustic source density on cross-correlated signals: implications for amplitude-based tomography in helioseismology, *Astrophys. J. Lett.* **725,** 313–318.

Dahlen, F., Hung, S.-H. & Nolet, G., 2000. Fréchet kernels for finite-frequency traveltimes—I. Theory, *Geophys. J. Int.* **141,** 157–174.

Fichtner, A., Kennett, B.L.N., Igel, H. & Bunge, H.-P., 2008. *Theoretical background for continental- and global-scale full-waveform inversion in the time-frequency domain, Geophys. J. Int.* **175,** 665–685.

Fichtner, A., Trampert, J., Cupillard, P., Saygin, E., Taymaz, T., Capdeville, Y. & Villasenor, A., 2013. Multi-scale full waveform inversion, *Geophys. J. Int.,* **194,** 534–556.

Froment, B., Campillo, M., Roux, P., Gouédard, P., Verdel, A. & Weaver, R.L., 2010. Estimation of the effect of nonisotropically distributed energy on the apparent arrival time in correlations, *Geophysics* **75,** SA85–SA93.

Halliday, D. & Curtis, A., 2008. Seismic interferometry, surface waves and source distribution, *Geophys. J. Int.* **175,** 1067–1087.

Hanasoge, S.M., 2014. Measurements and kernels for source-structure inversions in noise tomography, *Geophys. J. Int.,* in review.

Hanasoge, S.M., Birch, A., Gizon, L. & Tromp, J., 2011. The adjoint method applied to time-distance helioseismology, *Astrophys. J.* **738,** doi:10.1088/0004–637X/738/1/100.

Kimman, W. & Trampert, J., 2010. Approximations in seismic interferometry and their effects on surface waves, *Geophys. J. Int.* **182,** 461–476.

Lin, F.-C., Moschetti, M.P. & Ritzwoller, M.H., 2008. Surface wave tomography of the western United States from ambient noise: Rayleigh and Love wave phase velocity maps, *Geophys. J. Int.* **173,** 281–298.

Lobkis, O.I. & Weaver, R.L., 2001. On the emergence of the Green's function in the correlations of a diffuse field, *J. acoust. Soc. Am.* **110,** 3011–3017.

Luo, Y. & Schuster, G.T., 1991. Wave-equation traveltime inversion, *Geophysics* **56,** 645–653.

Sabra, K.G., Gerstoft, P.R. & Kuperman, W.A., 2005. Surface wave tomography from microseisms in Southern California, *Geophys. Res. Lett.* **32,** doi:10.1029/2005GL023155.

Sánchez-Sesma, F.J. & Campillo, M., 2006. Retrieval of the Green's function from cross correlation: the canonical elastic problem, *Bull. seism. Soc. Am.* **96,** 1182–1191.

Shapiro, N.M., Campillo, M., Stehly, L. & Ritzwoller, M., 2005. High resolution surface wave tomography from ambient seismic noise, *Science* **307,** 1615–1618.

Shen, W., Ritzwoller, M.H., Schulte, V. & -Pelkum, 2013. Crustal and uppermost mantle structure in the central U.S. encompassing the Midcontinent Rift, *J. geophys. Res.* **118,** 4325–4344.

Tape, C., Liu, Q., Maggi, A. & Tromp, J., 2010. Seismic tomography of the southern California crust based upon spectral-element and adjoint methods, *Geophys. J. Int.* **180,** 433–462.

Tromp, J., Luo, Y., Hanasoge, S. & Peter, D., 2010. Noise cross-correlation sensitivity kernels, *Geophys. J. Int.* **183,** 791–819.

Tsai, V.C., 2009. On establishing the accuracy of noise tomography traveltime measurements in a realistic medium, *Geophys. J. Int.* **178,** 1555–1564.

Wapenaar, K., 2004. Retrieving the elastodynamic Green's function of an arbitrary inhomogeneous medium by cross correlation, *Phys. Rev. Lett.* **93,** 254301-1–254301-4.

Woodard, M. F., 1997. Implications of localized, acoustic absorption for heliotomographic analysis of sunspots, *Astrophys. J.* **485,** 890–894.

SUPPORTING INFORMATION

Additional Supporting Information may be found in the online version of this article:

Movie S1. correlation_field_whitened.mp4
Movie S2. correlation_field_homogeneous.mp4
Movie S3. correlation_field_heterogeneous.mp4 (http://mnras.oxfordjournals.org/lookup/suppl/doi:10.1093/gji/ggu093/-/DC1).

Please note: Oxford University Press is not responsible for the content or functionality of any supporting materials supplied by the authors. Any queries (other than missing material) should be directed to the corresponding author for the article.